

RF Reflectometry for Readout of Charge Transition in a Physically Defined PMOS Silicon Quantum Dot

Sinan Bugu^{1*}, Shimpei Nishiyama¹, Kimihiko Kato², Yongxun Liu², Takahiro Mori² and Tetsuo Kodera^{1†}

¹*Tokyo Institute of Technology 2-12-1 Ookayama, Meguro-ku, Tokyo 152-8552, Japan*

²*Nanoelectronics Research Institute (NeRI), National Institute of Advanced Industrial Science and Technology (AIST), Central 2, 1-1-1 Umezono, Tsukuba, Ibaraki, 305-8568, Japan*

We have embedded a physically defined p-channel silicon MOS quantum dot (QD) device into an impedance transformer RC circuit. To decrease the parasitic capacitance and surpass the cutoff frequency of the device which emerges in MOS devices that have a top gate and act as RC low-pass filter, we fabricate a new device to reduce the device's top gate area from $400 \mu\text{m}^2$ to $0.09 \mu\text{m}^2$. Having a smaller top gate eliminates the cutoff frequency problem preventing the RF signal from reaching QD. We show that we have fabricated a single QD properly, which is essential for RF single-electron transistor technique. We also analyze and improve the impedance matching condition and show that it is possible to perform readout of charge transition at 4.2 K by RF reflectometry, which will get us to fast readout of charge and spin states.

1. Introduction

Quantum information processing based on silicon QDs is an appropriate platform for quantum computers thanks to its long coherence time¹⁾ and its compatibility with CMOS technology.^{2,3)} Particularly PMOS silicon QDs are convincing for the development of a spin-based qubit system since hole spins have smaller hyperfine interactions than that of electron spins and can be controlled only with an electric field as they have strong spin-orbit coupling (SOC).⁴⁻⁶⁾ Charge sensing technique, in which a capacitively coupled additional single QD (SQD) is required, has been used extensively to map out the charge states in QDs. While this technique is relatively easy to demonstrate since it only requires the devices to be properly fabricated, the integration time (t_{min}), which is the minimum time to discern and characterize the states, should also be considered. For a readout to be effective, the measurement needs to be faster than the relaxation time of the system. In quantum computing, in order to perform error correction, the

*E-mail: bugu.s.aa@m.titech.ac.jp

†E-mail: kodera.t.ac@m.titech.ac.jp

measurement time should be faster than the coherence time (T_2^*). For silicon qubits, t_{min} should be lower than $20 \mu s$.⁷⁾ Measurements done with charge sensing are restricted by the RC time constant of the charge sensor. Usually, these numbers are $R \lesssim 100 \text{ k}\Omega$ and C in the order of hundreds of pF that inhibit a charge sensor bandwidth to a few kilohertz or less.⁸⁾ Instead of performing a voltage and current tests, namely DC measurement, a so-called RF single-electron transistor (RF-SET) overcomes the low-frequency restriction by using an LC resonant tank circuit to measure RF waves, which are reflected from the SET.¹⁶⁾ This technique has been used to increase the bandwidth of SET and quantum point contact,^{17,18)} superconductor-insulator-normal thermometers and warrant rapid readout of charge sensor,^{19,20)} complex impedance measurement of quantum-dot circuits,^{23–29,31)} large gate two-dimensional systems,³²⁾ spin qubits,²²⁾ and nanomechanical resonators.²¹⁾

In this study, we use a physically defined PMOS silicon QD device to readout charge transition via RF reflectometry. The device we fabricated is a physically defined device, therefore it doesn't need gates to form QD^{10–12)} and it has less complexity. And since it is a p-channel device and has strong SOC it doesn't require additional structure for spin manipulation.^{13,14)} MOS device that has top gate behaves like low pass-filter and this precludes RF signal from reaching QD area. To tackle this disadvantage, we shrank the top gate area and fabricated a new device, as we explain in Section 3.1.

In the extended abstract for SSDM2020¹⁵⁾ we presented readout of charge transition via RF reflectometry. In this paper, we analyze and improve impedance matching condition in our setup, and investigate Coulomb diamond characteristic, which is vital to perform RF-SET, of the device we have fabricated by performing charge stability diagram. In addition, to better understand shrinking top gate area, schematic of the region around top gate is added.

2. Device fabrication

A scanning electron microscope (SEM) image and schematic of physically defined PMOS double QD (DQD) and SQD on undoped silicon-on-insulator (SOI) substrate are shown in Fig. 1(a), and 1(b), respectively. The dark and bright regions in Fig. 1(a) indicate the BOX layer of the structure, and the SOI layer, respectively. The device has three side gates (G_l , G_m , G_r) capacitively coupled to DQD and one side gate (G_{SQD}) capacitively coupled to SQD for controlling electrochemical potential. At first, a 40-nm thick SOI substrate is etched to form SQD, DQD, and side gates by reactive ion etching

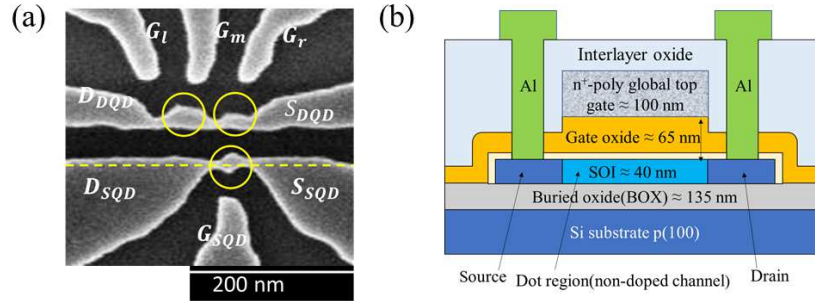


Fig. 1. Physically defined p-channel silicon MOS device. (a) Scanning electron microscope image of the device. Two QDs in DQD part and one QD in SQD part are circled in yellow. (b) Cross-sectional schematic of the device structure along yellow dashed line in (a).

technique after electron beam lithography. Next, following thermal passivation of the silicon surface, a 65-nm thick SiO_2 layer and a polysilicon top gate (TG) are deposited by low-pressure chemical vapor deposition technique. To shrink the conventional TG area from $400 \mu\text{m}^2$ to $0.09 \mu\text{m}^2$, TG is formed by electron beam lithography. Then, to create Ohmic contacts, boron ions are implanted into the SOI layer except for the part covered with the TG. Finally, forming gas annealing is performed to terminate dangling bonds. In this measurement, for simplicity, we used only an SQD.

3. Method and discussion

3.1 Experimental method

In this study, we use the RF-SET technique to readout charge transition in a physically defined PMOS silicon QD device. MOS devices that have TG can act as RC low-pass filter where R stands for the resistance of the lead of device, which is connected to the matching network via bonding wire and the gate capacitance for C_g . If the TG area is as large as a few decades of μm squares, i.e. our previously fabricated device has a TG area of $400 \mu\text{m}^2$,⁹⁾ it can have as low cutoff frequency as a few MHz or less (Eq. 1). This cutoff frequency prevents RF signal that has a frequency in excess of 80 MHz, where $1/f$ noise caused by charge motion is negligible,¹⁶⁾ applied through leads

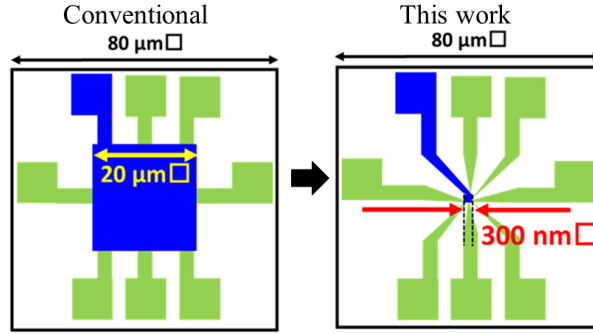


Fig. 2. Schematic of the region around QD with a square TG that has a side of $20\ \mu\text{m}$ (left) and $300\ \text{nm}$ (right). Blue and green regions denote TG and SOI, respectively. To surpass the cutoff frequency problem explained in the text, we reduced TG area from $400\ \mu\text{m}^2$ to $0.09\ \mu\text{m}^2$.

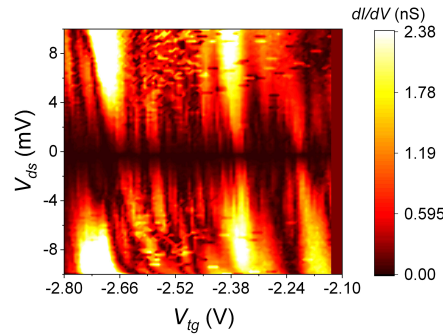


Fig. 3. Charge stability diagram. TG voltage, V_{tg} , and drain to source voltage, V_{ds} , are swept to obtain Coulomb diamonds. Current can flow out of the diamonds whereas it is blocked in the diamond regime where the first derivative of conductance, dI/dV , is minimum.

from reaching the QD. To surpass the cutoff frequency of the device, f_c , the TG area is reduced down from $400\ \mu\text{m}^2$ to $0.09\ \mu\text{m}^2$ as shown in Fig. 2. To perform RF-SET, we aimed at fabricating an SQD, which is expected to have a Coulomb diamond, the intrinsic property of an SQD.³⁰⁾ We performed a charge stability diagram by sweeping TG voltage and drain to source voltage and obtained the Coulomb blockade regime as in Fig. 3. Our measurement proves that the device we fabricated has an SQD characteristic as it has Coulomb diamonds. We then proceeded to reflectometry measurement. In the RF measurement, we first find the resonant frequency of the device when the bonding

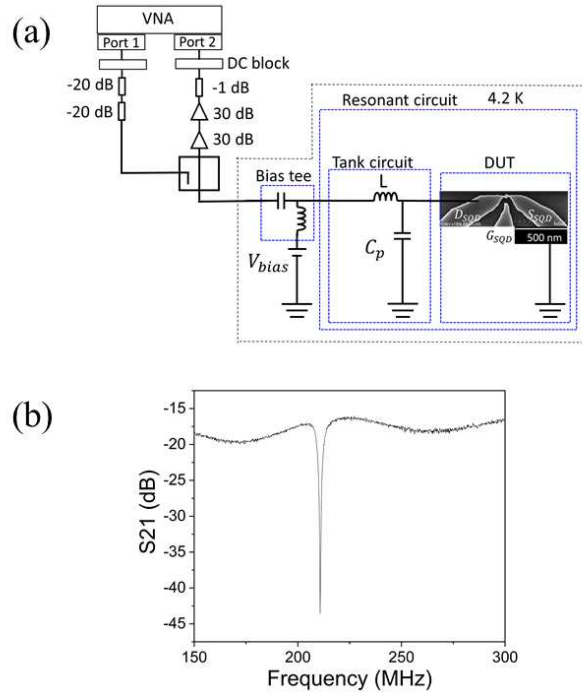


Fig. 4. (a) Measurement setup. Attenuated RF signal is sent through series LC resonant tank circuit to drain of single quantum dot (SQD) and reflected signal that is separated by directional coupler is amplified at room temperature before it reaches the second port of vector network analyzer. (b) S₂₁ as a function of frequency. Resonant frequency, $f_r = 210.875$ MHz, of the sample is shown when TG voltage is not applied.

wire is connected to the drain lead of SQD, which is mounted on an FR4 printed circuit board (PCB). We then send 210.875 MHz carrier frequency (f_o) in the time domain to the SQD through drain lead. Before the signal reaches the sample, it is attenuated with an -40 dB attenuator to avoid blowing up the device. Electron transition through SQD causes a change in amplitude of the reflected signal. The directional coupler sends the carrier signal down one line, and the reflected signal up another line. The reflected signal is transmitted through the directional coupler back up the carrier line. Afterward, the signal is amplified with room temperature amplifiers, which have a gain of 60 dB in total. Using a 2.2 μ H commercial inductor in a series LC resonant tank circuit in Fig. 4(a) gives us a resonant frequency, f_r of 210.875 MHz as shown in Fig. 4(b) from which we calculate the parasitic capacitance (C_p) as 0.258 pF by using Eq. (2).

$$f_c = \frac{1}{2\pi RC_g} \quad (1)$$

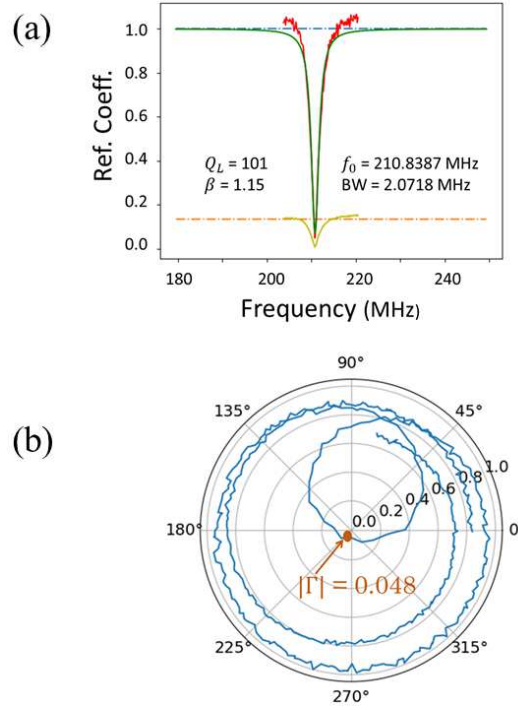


Fig. 5. Analysis of impedance matching. (a) Background noise is subtracted (red line) from Frequency vs Amplitude data shown in Fig. 4(b) and then fitted (green line) since it has a Lorentzian shape. The center frequency is 210.875 MHz and bandwidth of 3 dB regime (yellow line) is 2.0718 MHz. Loaded Q factor, Q_L , is found 101. The coupling strength, β , is 1.15 which is not far away from the best matching point where β is equal to 1 ($\beta = 1$). (b) Trace of reflected signal (blue line) is shown on polar plot. Reflection coefficient, Γ , is found to be 0.048. The best matching occurs where Γ crosses the origin of the polar plot ($\Gamma = 0$).

$$f_r = \frac{1}{2\pi\sqrt{LC_p}} \quad (2)$$

As we expected, this value, 0.258 pF, is much lower than that of obtained for the device with $400 \mu\text{m}^2$ TG area, which is 0.6 pF,⁹⁾ since it has a smaller TG area.

3.2 Analysis of impedance matching

To find out how good impedance matching we obtained in Fig. 2(b), we analyzed the matching conditions. We first subtracted the background noise. Then fit the impedance matching since it has a Lorentzian shape (see Fig. 5(a)). Using Eq. 3, we found the loaded quality factor $Q_L = 101$, which is the ratio between resonant frequency and bandwidth of 3 dB regime, that are 210.875 MHz and 2.071 MHz, respectively. The loaded quality factor is, literally, the quality factor of the matching network. Using Eq. 4 and Eq. 5, we found 1.15 for β , the coupling strength, which is the ratio of internal

(Q_{int}) and external (Q_{ext}) quality factors. Since β is greater than 1 ($\beta > 1$), the matching network is overcoupled, and there is a loss outside that prevents us from having the best impedance matching where β equals 1 ($\beta = 1$).³³⁾ We then analyzed the matching on the polar plot. In Fig. 5(b), the blue line shows the whole trace of the reflected signal. The best matching occurs where Γ (Eq. 6), reflection coefficient, crosses the origin of the polar axis ($\Gamma = 0$). At the best matching point, loaded impedance (Z_L) is equal to the characteristic impedance of the transmission line (Z_0), which has a typical value of 50 Ω .

$$Q = \frac{f_r}{BW} \quad (3)$$

$$\frac{1}{Q_L} = \frac{1}{Q_{ext}} + \frac{1}{Q_{int}} \quad (4)$$

$$\beta = \frac{Q_{int}}{Q_{ext}} \quad (5)$$

$$\Gamma = \frac{Z_L - Z_0}{Z_L + Z_0} \quad (6)$$

By having a Γ of 0.048, our impedance matching is close to the best matching point. It is worth noting that one could have a better impedance matching by doing some more circuit engineering but the present matching condition is enough to perform RF-SET.

3.3 RF readout measurement

After having the condition explained in the matching network in Section 3.2, we proceed to readout of charge transition by RF-SET technique. We sent a carrier frequency, f_o , of 210.875 MHz that has continuous waveform passing through the matching network. Amplitude change in reflected signal caused by charge transition between QD and the leads was mapped out by sweeping the TG voltage and analyzing S parameters, as shown in the upper panel of Fig. 6(a). At the same time, we performed standard I-V measurement, as shown in the lower panel of Fig. 6(a). Following, we performed a similar measurement by sweeping the side gate voltage while applying a constant negative voltage to the TG to form a channel between source and drain shown in Fig. 6(b). Coulomb peak characteristics are similar in both DC and RF measurements, meaning that we succeeded in the readout of charge transition via RF-SET technique

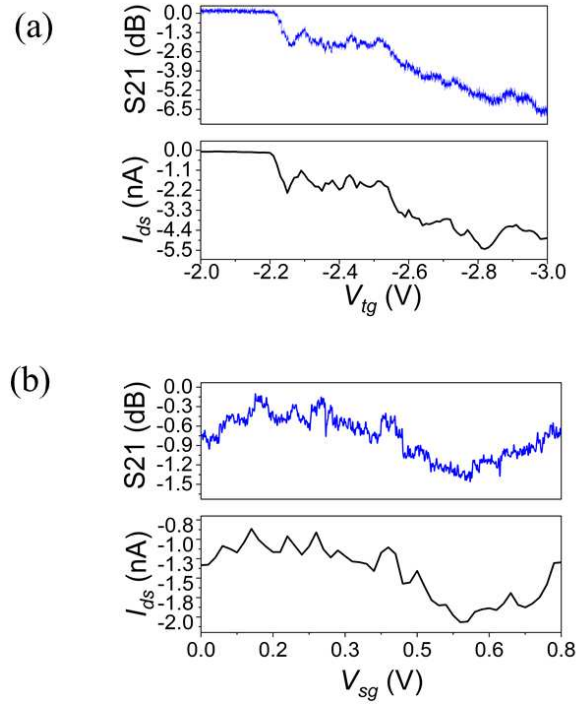


Fig. 6. Simultaneous measurements of RF and DC by sweeping TG (a) and side gate with constant TG voltage, $V_{tg} = -2.5$ V (b). Both TG and side gate work properly. RF and DC measurements are alike, implying that electron transition can be readout by RF reflectometry.

with improved device structure.

4. Conclusions

We have fabricated physically-defined PMOS QDs with smaller TG area and performed RF-SET measurements. Reducing TG area from $400 \mu\text{m}^2$ to $0.09 \mu\text{m}^2$ surpasses the cutoff frequency of the device, which behaves as an RC low pass filter, and permits the RF signal to reach QD area. We observed the Coulomb peaks via RF, and this result is in good agreement with what we obtained with DC measurement. This result shows us a route to fast spin readout in our future work.

Acknowledgment

S.B. thanks to M. Fernando Gonzalez-Zalba and David J. Ibberson for fruitful discussion. The part of this work was financially supported by JST CREST (JPMJ CR1675), JSPS KAKENHI (Grant Numbers JP18K18996 and JP20H00237), and MEXT Quantum Leap Flagship Program (Q-LEAP) Grant Number JPMXS0118069228.

References

- 1) M. Veldhorst, C.H. Yang, J.C.C. Hwang, W. Huang, J.P. Dehollain, J.T. Muhonen, S. Simmons, A. Laucht, F.E. Hudson, K.M. Itoh, and A. Morello, *Nature*, 526(7573), (2015).
- 2) B.M. Maune, M.G. Borselli, B. Huang, T.D. Ladd, P.W. Deelman, K.S. Holabird, A.A. Kiselev, I. Alvarado-Rodriguez, R.S. Ross, A.E. Schmitz, and M. Sokolich, *Nature*, 481(7381), (2012).
- 3) K. Takeda, J. Kamioka, T. Otsuka, J. Yoneda, T. Nakajima, M.R. Delbecq, S. Amaha, G. Allison, T. Kodera, S. Oda, and Tarucha, S., *Science advances*, 2(8), (2016).
- 4) B. Voisin, R. Maurand, S. Barraud, M. Vinet, X. Jehl, M. Sanquer, J. Renard, and S. De Franceschi, *Nano letters*, 16(1), (2016).
- 5) R. Li, F.E. Hudson, A.S. Dzurak, and A.R. Hamilton, *Nano letters*, 15(11), (2015).
- 6) R. Maurand, X. Jehl, D. Kotekar-Patil, A. Corna, H. Bohuslavskyi, R. Laviéville, L. Hutin, S. Barraud, M. Vinet, M. Sanquer, and S. De Franceschi, *Nature communications*, 7, 1375 (2016).
- 7) R.C.C. Leon, C.H. Yang, J.C.C. Hwang, J.C. Lemyre, T. Tanttu, W., Huang, K.W. Chan, K.W., K.Y. Tan, F.E. Hudson, K.M. Itoh, and A. Morello, *Nature communications*, 11, 797 (2020).
- 8) M. Manoharan, Y. Tsuchiya, S. Oda, and H. Mizuta, *Nano letters*, 8(12), 4648–4652 (2008).
- 9) Y. Yamaoka, K. Iwasaki, S. Oda, and T. Kodera, *Jpn. J. Appl. Phys*, 56(4S), 04CK07 (2017).
- 10) S. Mizoguchi, N. Shimatani, M. Makino, Y. Yamaoka, and T. Kodera, *Jpn. J. Appl. Phys*, 57(4S), 04FK03 (2018).
- 11) Y. Yamaoka, S. Oda, and T. Kodera, *Appl. Phys. Lett.* 109, 113109 (2016).
- 12) S. Hiraoka, K. Horibe, S. Ishihara, S. Oda, and T. Kodera, *Applied Physics Letters* 117, 074001 (2020).
- 13) E. Kawakami, P. Scarlino., D.R. Ward, F.R. Braakman, D.E. Savage, M.G. Lagally, M. Friesen, S.N. Coppersmith, M.A. Eriksson, and L.M.K. Vandersypen, *Nature Nanotechnology*. 9, 666 (2014).
- 14) J.T. Muhonen, J.P. Dehollain, A. Laucht, F.E. Hudson, R. Kalra, T. Sekiguchi, K.M. Itoh, D.N. Jamieson, J.C. McCallum, A.S. Dzurak, and A. Morello, *Nature*

- nanotechnology, 9(12), 986-991 (2014).
- 15) S. Bugu, S. Nishiyama, K. Kato, Y. Liu, T. Mori, and T. Kodera, SSDM2020I-6-02 (2020).
 - 16) R. J. Schoelkopf, P. Wahlgren, A. A. Kozhevnikov, P. Delsing, and D. E. Prober, Science 280, 1238 (1998).
 - 17) H. Qin and D. A. Williams, Appl. Phys. Lett. 88, 203506 (2006).
 - 18) M. C. Cassidy, A. S. Dzurak, R. G. Clark, K. D. Petersson, I. Farrer, D. A. Ritchie, and C. G. Smith, Appl. Phys. Lett. 91, 222104 (2007).
 - 19) D. R. Schmidt, C. S. Yung, and A. N. Cleland, Appl. Phys. Lett. 83, 1002 (2003).
 - 20) D. J. Reilly, C. M. Marcus, M. P. Hanson, and A. C. , Appl. Phys. Lett. 91, 162101 (2007).
 - 21) M. D. LaHaye, J. Suh, P. M. Echternach, K. C. Schwab, and M. L. Roukes, Nature (London) 459, 960 (2009).
 - 22) C. Barthel, M. Kjærgaard, J. Medford, M. Stopa, C. M. Marcus, M. P. Hanson, and A. C. Gossard, , Phys. Rev. B 81, 161308 (2010).
 - 23) K. D. Petersson, C. G. Smith, D. Anderson, P. Atkinson, G. A. C. Jones, and D. A. Ritchie, Nano Lett. 10, 2789 (2010).
 - 24) S. J. Chorley, J. Wabnig, Z. V. Penfold-Fitch, K. D. Petersson, J. Frake, C. G. Smith, and M. R. Bui-telaar, Phys. Rev. Lett. 108, 036802 (2012).
 - 25) M. Jung, M. D. Schroer, K. D. Petersson, and J. R. Petta, quantum dots, Appl. Phys. Lett. 100, 253508 (2012).
 - 26) M. D. Schroer, M. Jung, K. D. Petersson, and J. R. Petta, Phys. Rev. Lett. 109, 166804 (2012).
 - 27) J. I. Colless, A. C. Mahoney, J. M. Hornibrook, A. C. Doherty, H. Lu, A. C. Gossard, and D. J. Reilly, Phys. Rev. Lett. 110, 046805 (2013).
 - 28) M. F. Gonzalez-Zalba, S. Barraud, A. J. Ferguson, and A.C.Betz, Nat.Comm. 6, 6084 (2015).
 - 29) S. Schaal, I. Ahmed, J. A. Haigh, L. Hutin, B. Bertrand, S. Barraud, M. Vinet, C.M. Lee, N. Stelmashenko, J. W. A. Robinson, J. Y. Qiu, S. Hacoen-Gourgy, I. Siddiqi, M. F. Gonzalez-Zalba, and J. J. L. Morton Phys. Rev. Lett. 124, 067701 (2020).
 - 30) R. Hanson, L. P. Kouwenhoven, J. R. Petta, S. Tarucha, and L. M. K. Vandersypen. Rev. Mod. Phys. 79, 1217 (2007).
 - 31) N. Ares, F. J. Schupp, A. Mavalankar, G. Rogers, J. Griffiths, G. A. C. Jones, I.

- Farrer, D. A. Ritchie, C. G. Smith, A. Cottet, G. A. D. Briggs, and E. A. Laird
Phys. Rev. Applied 5, 034011 (2016).
- 32) L. J. Taskinen, R. P. Starrett, T. P. Martin, A. P. Micolich, A. R. Hamilton, M. Y.
Simmons, D. A. Ritchie, and M. Pepper. Review of Scientific Instruments 79, no.
12 (2008).
- 33) D. M. Pozar, Microwave Engineering, 4th ed. (John Wiley & Sons, Inc., 2012), p.
306.